Bull Earthquake Eng (2018) 16:5671–5696
https://doi.org/10.1007/s10518-018-0391-z

ORIGINAL RESEARCH PAPER

Copula-based seismic fragility assessment of base-isolated structures under near-fault forward-directivity ground motions

Tong Zhou[1] · **Ai-Qun Li**[1,2] · **Yi-Feng Wu**[2]

Received: 9 April 2018 / Accepted: 12 May 2018 / Published online: 23 May 2018

Abstract The seismic fragility of base-isolated structures subjected to near-fault forward-directivity ground motions is investigated. A general framework for deriving the system-level fragility curve is proposed, where the vulnerability contributions of multiple inter-related components to the overall system are incorporated. In this framework, the joint probabilistic seismic demand model (JPSDM) is established, where the joint probability distribution of multiple engineering demand parameters (EDPs), conditioned on the intensity measure (IM) level, is characterized via copula approach, and the sampling-based JPSDM, along with the capacity models of these components, is employed to generate the overall system fragility curves. This proposed framework is applied in the case study of a typical seismically-isolated RC frame structure, where the peak lateral displacement in the base-isolation layer and the maximum inter-story drift in the superstructure are considered as the two major component EDPs. The analysis results indicate that the combination of *t* copula, which is quantitatively identified as the best-fit copula function, and the conditional lognormal marginal distribution adequately captures the joint probability distribution of these two EDPs conditioned on the IM level. Moreover, the impact of different copulas selection on the system-level fragility varies depending on the relative fragility contributions of different components in the overall system.

Keywords Base-isolation · Near-fault · Seismic fragility · Copula approach

✉ Tong Zhou
zhoutong@seu.edu.cn

[1] School of Civil Engineering, Southeast University, Nanjing 210096, China

[2] Beijing Advanced Innovation Center for Future Urban Design, School of Civil and Transportation Engineering, Beijing University of Civil Engineering and Architecture, Beijing 100044, China

1 Introduction

Seismic isolation has been widely utilized in new construction and seismic rehabilitation of existing ones, as well as seismic performance enhancement of critical facilities. The introduction of base-isolation bearings can effectively decouple the superstructure from the intensive ground motion shakings and significantly reduce the seismic inertial forces transferred to it. Near-fault forward-directivity (NFFD) ground motions are characterized by short-duration, large-amplitude and long-period velocity pulses (Bray and Rodriguez-Marek 2004), whose periods may approximate to or even coincide with those of base-isolated structures, leading to excessive lateral displacement within the base-isolation layer and other unfavorable seismic responses in the superstructure. Therefore, there are plenty of experimental and analytical studies in the existing literature with respect to the seismic responses of base-isolated structures under NFFD ground motions, e.g., Alhan and Öncü-Davas (2016), Sato et al. (2011) and Shi et al. (2014). Given various sources of uncertainties pertaining to the structural system, ground motion characteristics, and the quantification of performance level, etc., a probabilistic approach, rather than a deterministic one, may provide a more comprehensive and rational framework for the seismic performance evaluation of this engineering system.

Probabilistic seismic risk assessment (PSRA) methodology has emerged as a robust approach for quantitatively measuring the potential seismic damage and loss consequences of engineering structures, which consists of three assessment modules, i.e., seismic hazard analysis, seismic fragility analysis, and seismic loss analysis (Baker 2015). Seismic fragility/vulnerability, serving as an indispensable part for the propagation of uncertainty in the PSRA, is defined as the probability of a structure or component exceeding a certain level of damage state for the given ground motion intensity level (Erdik 2017). Therefore, it is imperative to perform the seismic fragility analysis of base-isolation structures under NFFD ground motions. Component fragility curves are typically obtained using parametric or nonparametric approach. The lognormal cumulative distribution function is commonly utilized to define the parametric fragility function (Cornell et al. 2002; Zentner et al. 2017; Zhang and Huo 2009). The Gaussian kernel smoothing method is adopted by Noh et al. (2015) to derive the nonparametric fragility functions, and this method is developed without any assumption on the probability distribution but at the expense of robustness. Zentner (2017) proposed a fragility-generation framework from the basic definition of fragility function, namely, the cumulative conditional probability of the engineering demand parameters (EDPs) when knowing the intensity measure (IM) level.

As for the system-level fragility function, consideration of single critical component as representative of the system vulnerability was an option (Kim and Shinozuka 2004; Murcia-Delso and Shing 2012). Recently, the majority of existing studies just utilized the first-order or second-order reliability bounds to estimate the overall system fragility (Dezfuli and Alam 2017), whereas, the upper and lower bound provide conservative and unconservative estimates of the system fragility, respectively. Wu et al. (2016) utilized the product of conditional marginal method to directly derive the bridge system fragility. Wang et al. (2018) employed the multivariate lognormal probabilistic seismic demand model (PSDM) to account for the dependence among different EDPs, and this multivariate PSDM is used with the multidimensional performance limit state formula, which defines the failure domains of the system, to derive the overall fragility. Nielson and DesRoches (2007) derived the system-level fragility curves based on the conditional lognormal marginal distributions and the pairwise linear correlation coefficients between logarithms of these

EDPs. It should be noted that this method is essentially based on the Nataf transformation (Liu and Der Kiureghian 1986), and the main limitation lies in that the joint distribution of multiple demands are confined to the multivariate lognormal distribution (Lebrun and Dutfoy 2009).

This study aims to derive the system-level vulnerability of base-isolated structures under NFFD ground motions. To the best of the authors' knowledge, there is few studies in the existing literature associated with the application of copula theory in the field of seismic fragility assessment. This study is the first one that employs the copula approach to develop the general framework for generating fragility curves at the system level. In this framework, to account for the fragility contributions of various correlated components, the joint probabilistic seismic demand model (JPSDM) is constructed, which represents the joint probability distribution of multiple EDPs conditioned on the IM level. The key novelty of this investigation is that the copula theory is utilized to flexibly characterize the dependence among multiple EDPs and to further establish the sampling-based JPSDM. First, the basic methodology for developing the overall system fragility based on both the JPSDM and the associated capacity models of multiple components is presented; then, the copula theory for modeling the interrelation of multivariate random variables is briefly introduced; next, the sampling-based JPSDM is constructed through the copula approach; subsequently, the estimation of the failure probability of the overall system is illustrated; finally, the general procedure for generating system-level fragility curves is summarized. This general fragility-generation framework is then applied in the case study of a typical base-isolated RC frame, and the overall system fragility curves under different damage states are obtained. Comparisons between the system-level fragility curves and the component-level ones, as well as the first-order bounds, are made. Moreover, the impact of different copulas selection on the system-level fragility is investigated.

2 Methodology

Seismic fragility denotes the probability of the seismic demand (D) placed on a structure or component exceeding its associated capacity (C) defined at a damage state, conditional on a specific IM level, and is given as follows:

$$P_f = P[D \geq C \,|IM] \tag{1}$$

For the sake of developing the overall system fragility, the fragility function of individual component is derived firstly.

2.1 Component-level fragility function

The probabilistic seismic demand analysis (PSDA) and the incremental dynamic analysis (IDA) are the two commonly-utilized method to develop the component-level vulnerability (Zhang and Huo 2009). Given that the scaling of accelerograms to different IM levels in the IDA method may induce the bias of structural responses (Luco and Bazzurro 2007) and requires extensive computational effort, the PSDA method is utilized herein.

In the PSDA method, the development of component-level fragility function entails the convolution of the PSDM, which represents the probability distribution of the EDP conditioned on the IM level, with the probabilistic capacity model (or limit/damage state model) of each component, which is representative of a measure of its functionality level. As suggested by Cornell et al. (2002), for the ith component, the selected EDP and IM are

all assumed to be lognormally distributed, and the linear regression analysis is utilized to relate the natural logarithm of EDP to that of IM:

$$\ln(EDP_i) = \underbrace{\ln(a_i) + b_i \cdot \ln(IM)}_{\ln(S_{d,i})} + e_i, \quad i = 1, \ldots, n \tag{2}$$

where $\ln(S_{d,i})$ ($=\ln(a_i)+b_i \cdot \ln(\mathrm{IM})$) is the conditional mean of EDP_i as a function of IM; a_i and b_i are the regression parameters; the residual term e_i is considered to be normally distributed with zero mean and the standard deviation, $\beta_{EDP|\mathrm{IM},i}$:

$$\beta_{EDP/IM,i} = \sqrt{\frac{\sum_{j=1}^{N} (\ln(edp_j) - \ln(S_{d,i}))^2}{N-2}} \tag{3}$$

where edp_j is the jth recorded value of EDP_i under consideration ($j=1, \ldots, N$). The expression of Eq. (3) implies that the constant variance of $\ln(EDP_i)$ is assumed over the entire IM range. Therefore, the generic functional form of PSDM is given as follows:

$$P\left[EDP_i \geq d_i | IM\right] = 1 - \Phi\left(\frac{\ln(d_i) - \ln(S_{d,i})}{\beta_{EDP|IM,i}}\right) \tag{4}$$

where $\Phi()$ is the standard normal cumulative distribution function (CDF); d_i is the demand value defined at a specific limit state.

The capacity model (limit/damage state model) for individual component is quantified in terms of the corresponding EDP and is inherent with uncertainty. In general, the lognormal distribution function is utilized to describe the variability in the capacity model, and the distribution parameters, i.e., the median S_c and the dispersion β_c, are typically determined based on analytical, experimental results, etc.

Given that the PSDM and the limit state model are both lognormally distributed, the fragility function for each component, as stated in Eq. (1), can be calculated as follows:

$$P_i[D > C|IM] = \Phi\left[\frac{\ln\left(S_{d,i}/S_{c,i}\right)}{\sqrt{\beta^2_{EDP|IM,i} + \beta^2_{c,i}}}\right] \tag{5}$$

Substituting Eq. (2) into Eq. (5), the fragility function of each component can be simplified as

$$P_i[D > C|\, IM] = \Phi\left[\frac{\ln(IM) - \lambda_i}{\zeta_i}\right] \tag{6}$$

where the median $\lambda_i = [\ln(S_{c,i}) - \ln(a_i)]/b_i$, and the dispersion $\zeta_i = \sqrt{\beta^2_{EDP|IM,i} + \beta^2_{c,i}}/b_i$.

2.2 System-level fragility function

As elucidated in Sect. 2.1, PSDMs of various components just describe the probability distribution of each EDP conditioned on the IM level, and are incapable of capturing the correlations among multiple EDPs, resulting in the inadequacy of deriving the system-level fragility. Therefore, the methodology for generating fragility curves at the system level that accounts for

the vulnerability contributions of multiple correlated components through the copula approach is proposed in the following.

2.2.1 Basic framework

In the proposed methodology, the development of system-level fragility is facilitated by establishing the JPSDM, which represents the joint probability distribution of multiple correlated EDPs conditioned on the IM level. Given that the failure domains of JPSDM are dominated by capacity models of these considered components, which are inherent with significant uncertainty, the direct calculation of system-level vulnerability by the integration of the JPSDM over the entire failure domains is impractical. Moreover, the overall structure can be reasonably regarded as a serial system, in which the failure of any individual segment results in the system failure, i.e., $E_{sys} = \bigcup_{i=1}^{n} E_{comp,\,i}$, where $\bigcup()$ is the union operator; E_{sys}, and $E_{\mathrm{comp},i}$ are the failure event of the system and the ith component, respectively. Therefore, the development of sampling-based JPSDM, the role of which is to provide a large set of simulated samples for multiple interrelated EDPs under each level of IM, is used with the associated capacity models of these components to statistically estimate the system-level fragility.

Since copula function provides a flexible approach for modeling the correlation among multivariate random variables, the copula concept is briefly introduced to facilitate the understanding of its advantage in representing the interrelation between random variables and the JPSDM is then established via this approach.

2.2.2 Copula theory

Copula function can flexibly characterize the nonlinear interrelationship of multivariate random variables and has been extensively employed in finances (Eckernkemper 2018), hydrological engineering (Tosunoglu and Singh 2018), geotechnical engineering (Wang and Li 2017), etc. The critical issues with respect to characterizing, measuring and modeling the dependence structure of random variables through copulas are briefly introduced in the following.

2.2.2.1 Definition Copula function $C(u_1, \ldots, u_n)$ is the n-dimensional CDF on a unit hypercube $[0, 1]^n$, whose marginal distributions U_i $(i=1, \ldots, n)$ follow uniform distributions on [0, 1], and is given as follows (Nelsen 2006):

$$C(u_1, \ \ldots, \ u_n) = P\left[U_1 \le u_1, \ \ldots, \ U_n \le u_n\right] \tag{7}$$

in which u_i is a sample of U_i. According to Sklar's theorem (Sklar 1959), the joint CDF of a random vector $(X_1, \ldots, X_n)$ can be described by a copula function in terms of their marginal distributions, $F_i(X_i)$ $(i=1, \ldots, n)$, and is expressed as follows:

$$\begin{aligned} F(x_1, \ldots, x_n) &= P\left[X_1 \le x_1, \ldots, X_n \le x_n\right] = P\left[F_1(X_1) \le F_1(x_1), \ldots, F_n(X_n) \le F_n(x_n)\right] \\ &= P\left[U_1 \le F_1(x_1), \ldots, U_n \le F_n(x_n)\right] = C\left(F_1(x_1), \ldots, F_n(x_n)\right) = C\left(u_1, \ldots, u_n\right) \end{aligned} \tag{8}$$

in which $U_i = F_i(X_i)$ and follows the uniform distribution on [0, 1]; $u_i = F_i(x_i)$ is the corresponding sample value. As implied in Eq. (8), one of salient advantages of copula function is that the modeling of the marginal distribution and the dependence structure can be separated.

The corresponding joint probability density function (PDF) is expressed as

$$f(x_1, \ldots, x_n) = c(u_1, \ldots, u_n) \cdot \prod_{i=1}^{n} f_i(x_i) \tag{9}$$

where $f_i(x_i)$ is the marginal PDF of x_i; and the copula density function $c(u_1, \ldots, u_n)$ is given as follows:

$$c(u_1, \ldots, u_n) = \frac{\partial^n C(u_1, \ldots, u_n)}{\partial u_1 \ldots \partial u_n} \tag{10}$$

As listed in Table 1, the widely-used copula families consist of elliptical copulas and Archimedean copulas. Other families of copulas and their separate functional forms can be found in Nelsen (2006).

Gaussian copula corresponds to a limiting case of t copula when the degrees-of-freedom parameter v approaches infinity. And the remarkable merit of t copula is that it can characterize the symmetric upper and lower tail dependence of random variables, whereas, the Gaussian copula does not exhibit any tail dependence.

The generic form of the Archimedean family of copulas is expressed as follows:

$$C(u_1, \ldots, u_n) = \varphi_\theta^{-1}\left(\varphi_\theta(u_1), \ldots, \varphi_\theta(u_n)\right) \tag{11}$$

where $\varphi_\theta(t)$ is the generator function, and $\varphi_\theta^{-1}(t)$ is the pseudo-inverse of $\varphi_\theta(t)$. The main discrepancy among the three common Archimedean copulas lies in the adequacy of modeling tail dependence: the Gumbel copula is upper tail dependent, and the Clayton copula is lower tail dependent, whereas, the Frank copula captures non tail dependence.

The behavior of tail dependence is pivotal to the dependent phenomena of extreme events, and the coefficients of upper and lower tail dependence, λ_U and λ_L, for a bivariate variable (X_i, X_j) are defined as (Nelsen 2006)

$$\begin{aligned} \lambda_U &= \lim_{q \to 1^-} P[X_i > F_i^{-1}(q) | X_j > F_i^{-1}(q)] \\ \lambda_L &= \lim_{q \to 0^+} P[X_i < F_i^{-1}(q) | X_j < F_j^{-1}(q)] \end{aligned} \tag{12}$$

Table 1 Summary of frequently-used n-dimensional copula functions

Copula	$C(u_1, \ldots, u_n)$	Generator function $\varphi_\theta(t)$	Range of parameter
Elliptical			
Gaussian	$\Phi_\rho(\Phi^{-1}(u_1), \ldots, \Phi^{-1}(u_n))$	–	$[-1, 1]$
t	$t_{\rho,v}(t_v^{-1}(u_1), \ldots, t_v^{-1}(u_n))$	–	$[-1, 1]$
Archimedean			
Gumbel	$\exp\left(-\left(\sum_{i=1}^n (-\ln u_i)^\theta\right)^{1/\theta}\right)$	$(-\ln t)^\theta$	$[1, \infty)$
Clayton	$\left(\sum_{i=1}^n u_i^{-\theta} - 1\right)^{-1/\theta}$	$t^{-\theta} - 1$	$[-1, \infty)\backslash\{0\}$
Frank	$-\frac{1}{\theta} \ln\left(1 + \frac{\prod_{i=1}^n (e^{-\theta u_i} - 1)}{(e^{-\theta} - 1)^{n-1}}\right)$	$-\ln \frac{e^{-\theta t} - 1}{e^{-\theta} - 1}$	$(-\infty, \infty)\backslash\{0\}$

$\Phi_\rho()$ is the n-dimensional standard Gaussian distribution with the correlation matrix $\boldsymbol{\rho}$; Φ is the univariate standard Gaussian distribution function; $t_{\rho,v}$ is the n-dimensional t distribution with the correlation matrix $\boldsymbol{\rho}$ and the degrees-of-freedom parameter v; t_v is the univariate t distribution function with v

where $F_i(x_i)$ and $F_j(x_j)$ are the CDFs of x_i and x_j, respectively; and q is the corresponding quantile value. The relationship between λ_U, λ_L and the copula function is given as follows:

$$\lambda_U = \lim_{t\to 1^-} \frac{1-2t+C(t,t;\theta)}{1-t}$$
$$\lambda_L = \lim_{t\to 0^+} \frac{C(t,t;\theta)}{t} \tag{13}$$

Substituting specific functional forms of these commonly-used copulas into Eq. (13), the corresponding upper and lower tail coefficients are listed in Table 2.

2.2.2.2 Estimation of copula parameters The maximum pseudo-likelihood estimation (MPLE) is considered as a robust choice to estimate the copula parameters (Kim et al. 2007), and the log-likelihood function $L(\theta)$ is expressed as follows:

$$L(\theta) = \ln\left(\prod_{i=1}^{s} c\left(\tilde{u}_{i,1},\ldots,\tilde{u}_{i,n};\theta\right)\right) = \sum_{i=1}^{s} \ln c\left(\tilde{u}_{i,1},\ldots,\tilde{u}_{i,n};\theta\right) \tag{14}$$

where n denotes the number of copula dimensions; s is the sample size; $\left(\tilde{u}_{i,1},\ldots,\tilde{u}_{i,n}\right)$ is the pseudo-observation of $(x_{i,1}, \ldots, x_{i,n})$ $(i=1, \ldots,s)$ and are calculated as follows (Genest and Favre 2007): $\tilde{u}_{i,j} = rank(x_{i,j})/(s+1)$, where rank$(x_{i,j})$ is the rank of $x_{i,j}$ among $(x_{1,j}, \ldots, x_{s,j})$ $(j=1, \ldots, n)$ in ascending order. The copula parameters are estimated by

$$\hat{\theta}_{ML} = \arg\max_{\theta\in\Theta} L(\theta) \tag{15}$$

where Θ is the considered range of θ.

The inversion of Kendall's τ method is another popular semi-parametric method for estimating copula parameters in multivariate elliptical copulas and bivariate Archimedean copulas. Kendall correlation coefficient τ is a measure of dependence and is defined as

$$\tau(X_i, X_j) = P\left[(X_i-\tilde{X}_i)(X_j-\tilde{X}_j)>0\right] - P\left[(X_i-\tilde{X}_i)(X_j-\tilde{X}_j)<0\right] \tag{16}$$

Table 2 Measures of dependence for widely-used bivariate copulas

Copula	Relationship between the copula parameter and the Kendall's τ	Upper tail coefficient λ_U	Lower tail coefficient λ_L
Elliptical			
Gaussian	$\rho = \sin(\pi\,\tau/2)$	0	0
t	$\rho = \sin(\pi\,\tau/2)$	$2-2t_{v+1}\left(\frac{\sqrt{v+1}\sqrt{1-\rho}}{\sqrt{1+\rho}}\right)$	
Archimedean			
Gumbel	$\theta = 1/(1-\tau)$	$2-2^{1/\theta}$	0
Clayton	$\theta = 2\tau/(1-\tau)$		$0\,2^{-1/\theta}$
Frank	$\tau = 1-\frac{4}{\theta}+\frac{4}{\theta^2}\int_0^\theta \frac{t}{\exp(t)-1}dt$		0 0

$t_{v+1}()$ is the univariate t distribution with the degrees-of-freedom parameter $v+1$

in which $(\tilde{X}_i, \tilde{X}_j)$ is an independent copy of (X_i, X_j).

For multivariate elliptical copulas, the one-to-one mapping between the Kendall's τ and the copula parameter, i.e., the element in the linear correlation matrix $\boldsymbol{\rho}$, is given as follows:

$$\tau(X_i, X_j) = \frac{2}{\pi} \sin^{-1}\left(\rho(X_i, X_j)\right) \tag{17}$$

For bivariate Archimedean copulas, the general relationship between the Kendall's τ and the generator function $\varphi_\theta()$ is given as follows:

$$\tau = 1 + 4\int_0^1 \frac{\varphi_\theta(t)}{\varphi_\theta^{-1}(t)}\, dt \tag{18}$$

Substituting the specific form of $\varphi_\theta(t)$ for each Archimedean copula into Eq. (18), the resulting expression is presented in Table 2. In the case of small samples characterized by a low degree of dependence, the inversion of Kendall's τ method is more efficient by comparison with the MPLE (Kojadinovic and Yan 2010).

2.2.2.3 Identification of the best-fit copula Once copula parameters have been estimated, the following step is to select the copula that best represents the dependence of the considered variables. In this study, the goodness-of-fit of each copula function is examined in terms of the Akaike Information Criterion (AIC) (Akaike 1974) or the Bayesian Information Criterion (BIC) (Schwarz 1978), which are given as follows:

$$\mathrm{AIC} = -2\sum_{i=1}^{s} \ln c(u_{1i}, \ \ldots, \ u_{ni}) + 2k \tag{19}$$

$$\mathrm{BIC} = -2\sum_{i=1}^{s} \ln c(u_{1i}, \ \ldots, \ u_{\mathrm{n}i}) + h \ln s \tag{20}$$

where $\ln c(u_{1i}, \ldots, u_{ni})$ is the maximized log-likelihood values of copula density function (Eq. (14)); h is the number of copula parameters. A copula function corresponding to the minimum AIC or BIC value is regarded as the best-fit copula among these candidate copulas.

2.2.2.4 Copula-based sampling method (CBSM) The role of CBSM (Wu 2013) is to generate a large ensemble of simulated samples of the n-variate random vector $(u_1, \ldots, u_n)$ on the unit hypercube $[0,1]^n$ based on the conditional inverse method (Rosenblatt 1952) for the specific copula function, therefore, the dependence structure of the original data set can be reconstructed. By virtue of the CBSM, the failure probability of a stochastic event can be statistically estimated by the ratio of the number of failure samples, n_f, to that of the total generated samples, n_t, i.e., $P_f = n_f/n_t$. In general, when n_t is greater than $100/P_f$, the accuracy can be satisfactory.

The analytical work associated with the estimation of copula parameters, the quantitative identification of best-fit copula, and the copula sample realizations, is performed

based on Matlab (MathWorks 2018) and the package 'copula' (Yan 2007) in the statistical software R (R Development Core Team 2018).

2.2.3 Development of sampling-based JPSDM

The role of sampling-based JPSDM is to obtain sample realizations of multiple correlated EDPs for each level of IM. Since the copula function is rank-dependent and is invariant against strictly monotonic transformation of random variables, the dependence structure among $\ln(\mathrm{EDP}_i)$ ($i=1, \ldots, n$) modeled by the copula approach is the same as that among their corresponding residual terms e_i in each PSDM [Eq. (2)].

First, as for the marginal distribution modeling, $\ln(\mathrm{EDP}_i)$ follow normal distribution (namely, EDP_i follow lognormal distribution), which is due to the fact that the residual term e_i in each PSDM is required to satisfy the normal requirement underlying the linear regression analysis. At each level of IM, the mean of $\ln(\mathrm{EDP}_i)$ is the corresponding conditional mean of each PSDM, i.e., $\ln(S_{d,i}) = \ln(a_i) + b_i \cdot \ln(\mathrm{IM})$, and the standard deviation of $\ln(\mathrm{EDP}_i)$ is equal to that of the residual term e_i in each PSDM, i.e., $\beta_{\mathrm{EDP|IM},i}$, which is constant in the whole IM range. Therefore, it can be inferred that $\ln(\mathrm{EDP}_i)$ follows the normal distribution with the mean $\ln(S_{d,i})$, which is conditioned on the IM level, and the constant standard deviation $\beta_{\mathrm{EDP|IM},i}$.

Then, the dependence among residual terms e_i ($i=1, \ldots, n$) of each PSDM is modeled via the copula approach, and the best-fit copula is quantitatively identified in terms of AIC or BIC values.

Finally, according to the best-fit copula function for ($e_1, \ldots, e_n$), a large set of sample realizations of ($u_1, \ldots, u_n$) on the unit hypercube $[0, 1]^n$ can be generated based on the CBSM, and the simulated samples of ($\ln(\mathrm{EDP}_1), \ldots, \ln(\mathrm{EDP}_n)$) can be obtained by the isoprobabilistic transformation based on their respective marginal distributions, i.e., $\ln(\mathrm{EDP}_i) = \Phi_i^{-1}(u_i)$ ($i=1, \ldots, n$), where $\Phi_i()$ is the separate CDF of the conditional normal marginal function for $\ln(\mathrm{EDP}_i)$. Therefore, random samples of multiple correlated EDPs ($\mathrm{EDP}_1, \ldots, \mathrm{EDP}_n$), under each IM level can be easily obtained.

Figure 1 shows the flowchart for sample realizations of multiple correlated EDPs under each level of IM. It is obvious that this method reasonably accounts for the nonlinear dependence among multiple EDPs in the whole system.

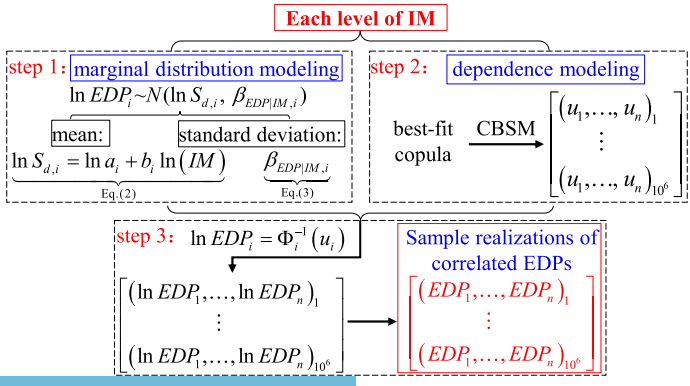

Fig. 1 Flowchart for sample realizations of multiple correlated EDPs under each IM level

2.2.4 The failure probability of the system

The sampling-based JPSDM, along with the capacity models of multiple considered components, is utilized to estimate the system-level failure probability, $P_{f,\mathrm{sys}}$, under each level of IM. Specifically, 10^6 sample realizations of both the JPSDM (i.e., samples of multiple correlated EDPs (EDP_1, EDP_2, …, EDP_n), as presented in Fig. 1) and the associated capacity models [i.e., capacity samples of different components (C_1, C_2, …, C_n)] for a specific IM level are generated. Under the assumption of a serial system, the probability of the demand placed on the system exceeding its capacity for this IM level is estimated, as presented in Fig. 2. With the increasing level of IM, a set of sample values for (IM, $P_{f,\mathrm{sys}}$) are obtained.

2.2.5 General procedure

The basic procedure for developing the system-level fragility curve is summarized as follows:

(1) Establishing analytical model for the target structure and providing a suite of ground motions that represents salient characteristics of the region being considered;
(1) Selecting suitable IM and EDP_i ($i=1, \ldots, n$) in the whole system, and determining the corresponding capacity models of different components;
(3) Nonlinear time history analyses are performed based on the established analytical model and the suite of ground motions, where the IM and different EDPs results are recorded;
(4) For each EDP_i, the regression analysis is performed based on the recorded results to obtain the regression parameters (a_i, b_i, and $\beta_{\mathrm{EDP|IM},i}$) in each PSDM, and the marginal distribution conditioned on the IM level is established (Sect. 2.2.1);
(5) The best-fit copula for characterizing the dependence among the residual term e_i ($i=1$, …, n) of each PSDM is quantitatively identified based on the metrics of AIC and BIC (Sect. 2.2.2.3);
(6) The sampling-based JPSDM is established based on the best-fit copula and the fitted conditional marginal distribution for a specified IM level (Sect. 2.2.3);

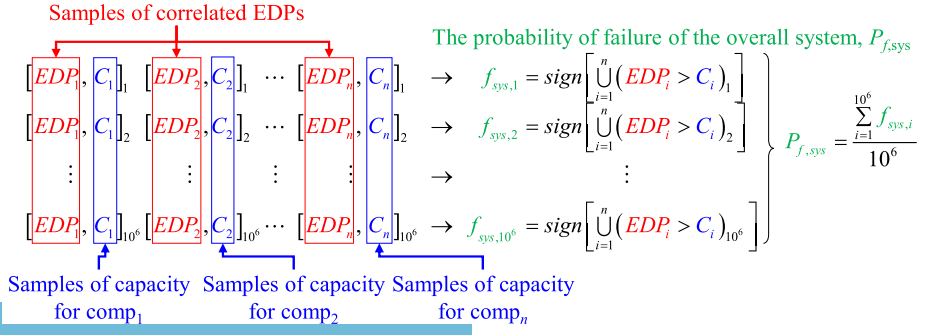

Fig. 2 Flowchart for the estimation of the failure probability of the system for a given IM level

(7) The failure probability of the whole system, $P_{f,\mathrm{sys}}$, for a given IM level is calculated by virtue of both the established JPSDM and capacity models of these components (Sect. 2.2.4);
(8) The step (7) is repeated for the increasing level of IM, resulting in a set of sample values for (IM, $P_{f,\mathrm{sys}}$);
(9) Analogous to component-level fragility function presented in Eq. (6), system-level fragility function is also assumed to follow lognormal distribution:

$$P\left[DS|IM\right] = \Phi\left[\frac{\ln(IM) - \lambda_{sys}}{\zeta_{sys}}\right] \tag{21}$$

where the median λ_{sys} and the dispersion ζ_{sys} are obtained by the maximum likelihood estimation (MLE) based on the set of (IM, $P_{f,\mathrm{sys}}$) data. Figure 3 illustrates a schematic of the general framework for the development of overall system fragility curves.

3 Seismic fragility analysis of seismically-isolated structures

This proposed methodology for generating system-level fragility curves is employed in the case of a typical based-isolated RC frame subjected to NFFD ground motions. For brevity, only the effect of record-to-record variability is considered and the uncertainty in the structural model is neglected.

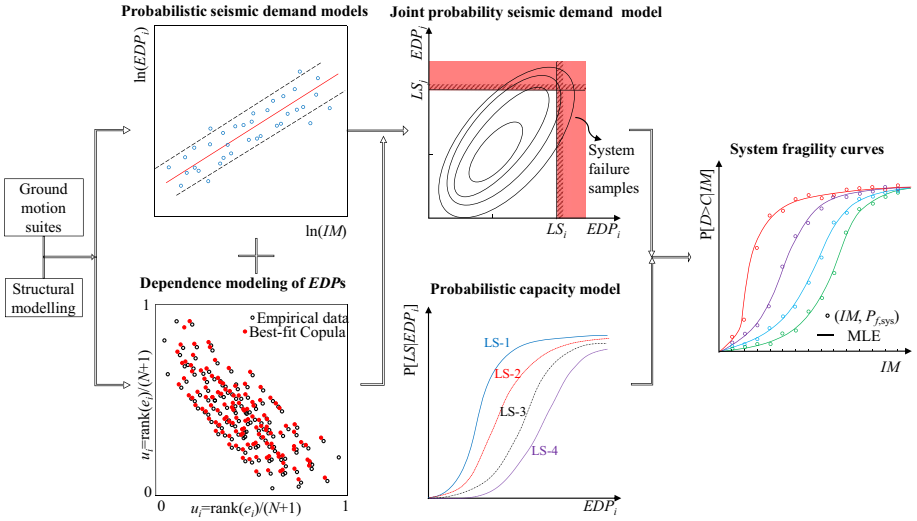

Fig. 3 The general framework for developing copula-based system fragility curves

3.1 Base-isolated structure description and analytical modeling

3.1.1 The layout of base-isolated structure

A typical six-story base-isolated RC frame is designed according to the current Chinese seismic code (GB 50011-2010) (Ministry of Housing and Urban–Rural Development of the People's Republic of China 2010). The main considered design factors include: the site condition [medium-stiff soil (site-class II)], the design earthquake group (1st group); high-intensity area (the fortification intensity is 8, and the design basic seismic acceleration is 0.2 g); moreover, based on the provisions in the Clause 12.2.2.2 of this code, the impact of near-fault effects is incorporated by multiplying the design response spectrum by the near-field affected factor over the whole range of periods, which is set to 1.5 herein. The calculated design spectrum is presented in Fig. 5a. Lead-rubber bearing (LRB) is selected as the bearing type, and the plan view and elevation view of this frame structure are illustrated in Fig. 4a, b, respectively. In view of the regularity and symmetry of this structure, the plane frame is selected as the analytical object.

Table 3 provides the information on the reinforcement details, the section geometry of columns and beams. And the design parameters of LRBs are presented in Table 4. It is noted that the enhanced reinforcement details in the base-isolation layer, which ensures this layer to behave as a rigid diagram, is beneficial to the effectiveness of base isolation.

3.1.2 The analytical model

The analytical model is established in OpenSees (McKenna et al. 2000). The superstructure is modeled using the nonlinear force-based element with fiber-defined cross-section. The uniaxial Menegotto-Pinto model (Filippou et al. 1983) is employed to represent the steel material, with the yield strength and the modulus of elasticity equal to 335 MPa and 2.1×10^5 MPa, respectively. The Kent-Park model with linear tensile strength (Mohd

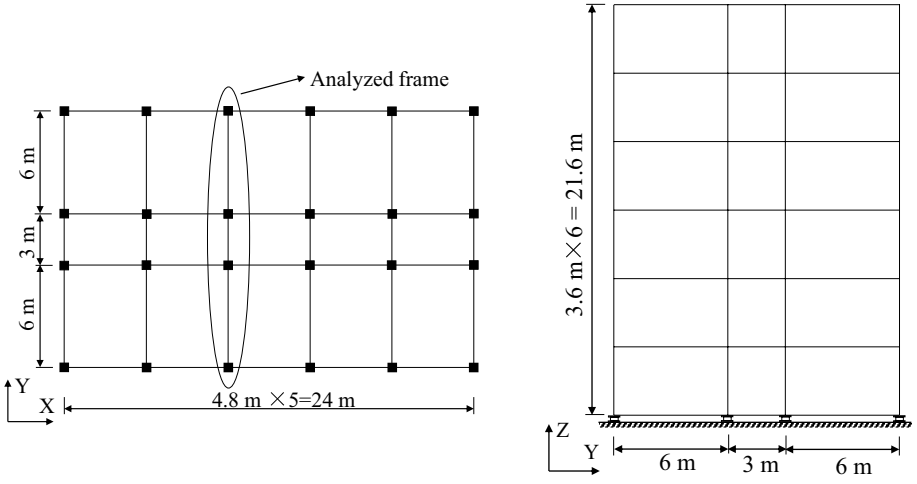

Fig. 4 Schematic of the seismically-isolated RC frame: **a** plan view, **b** elevation view

Table 3 The reinforcement details, the section geometry of beams and columns

Member	Section		Longitudinal reinforcement		Hooped reinforcement
	Width (mm)	Height (mm)	Top	Bottom	
Superstructure edge beam	300	500	4Φ18	2Φ25	Φ8@150
Superstructure middle beam	300	500	4Φ18	2Φ20	Φ8@150
Isolation layer beam	300	600	4Φ20	4Φ25	Φ8@100
column	500	500	8Φ18		Φ8@150

Table 4 Parameters of LRBs in current study

Parameter	Notation	Unit	Value
Outer diameter	D	mm	400.0
Lead-core diameter	d	mm	80.0
Thickness of rubber layers	$n_r \times t_r$	mm	16×5
Thickness of steel shims	$n_s \times t_s$	mm	15×3
Thickness of end plate	$n_p \times t_p$	mm	2×25
Shear modulus	G	MPa	0.3
First shape factor	S_1	–	20.0
Second shape factor	S_2	–	5.0
Characteristic strength	Q_d	kN	50.0
Post-yield stiffness	K_d	kN/m	500.0

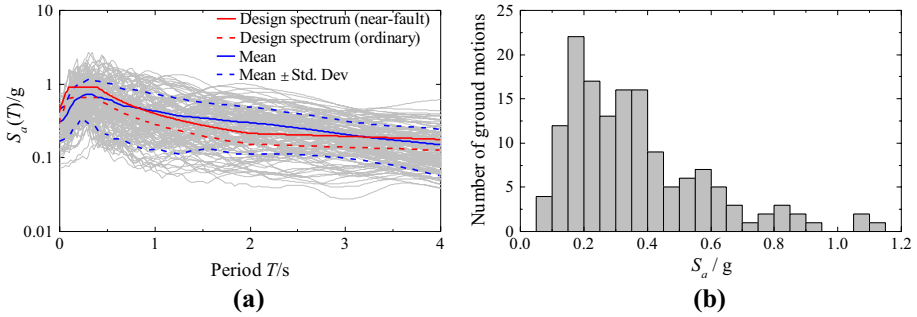

Fig. 5 The information of this suite of input ground motions: **a** response spectra of the ground motion suite and the design spectrum; **b** the distribution of S_a values of the suite ground motions

Yassin 1994) is used to describe the concrete material, and the compression strength and the modulus of elasticity are 24.75 MPa and 2.98×10^4 MPa, respectively. The confinement effect of the concrete section, which is manifested by the increase of the maximum compressive stress and the ultimate strain, is incorporated based on the reinforcement detailing.

LRBs are modeled using the ElastomericBearing element (Schellenberg et al. 2015). Since the first shape factor $S_1 = 20$ and the second shape factor $S_2 = 5$, the failure mode of LRBs under combined compression and shear is dominated by the shear failure, rather than the critical buckling behavior (Montuori et al. 2016); moreover, the reduced compression stiffness due

to lateral offset is still high in the considered range of horizontal displacements (Warn et al. 2007). Therefore, the linear model with constant stiffness (Warn et al. 2007) in assigned in the compressive direction. Given that the quantitative measures of different damage states for bearings in tension based on experimental or analytical results are relatively scare (Kumar et al. 2015), the tensile failure of bearings is not incorporated, and the constant tension stiffness that equals the compression stiffness is assumed in the tensile direction. The Bouc-Wen model is utilized to characterize the nonlinear hysteretic behavior in the horizontal direction. The hardening component parameters α_1, α_2, and μ are separately assumed to be 0.1, 0, and 2 (Buckle et al. 2006). The parameters γ and β control the shape of the hysteretic loop and are taken as 0.5 and 0.5, respectively (Casciati 1989; Constantinou et al. 1990; Huang 2002); the parameter η dominates the sharpness of the transition from elastic to inelastic state and is assumed to be 2 (Huang 2002).

Moreover, 5% Rayleigh damping is imposed in the structural system. The fundamental-mode period of the non-isolated frame and the seismically-isolated one are 0.657 and 1.126 s, respectively. Obviously, the introduction of base-isolation bearings effectively lengthens the natural period of engineering structures and, as a result, reduces the seismic inertial forces transferred to the superstructure.

3.2 Ground motion suite

In light of the scarcity of recorded NFFD ground motions, a scenario-based stochastic ground motion model developed by Zhou et al. (2018) is employed herein. This stochastic model is established in the strongest pulse orientation (Shahi and Baker 2014) and combines the velocity pulse part, which is represented by Gabor wavelet model (Dickinson and Gavin 2011), and the high-frequency content, which is characterized by the modulated filtered white-noise model (Rezaeian and Der Kiureghian 2008). This scenario-based model effectively captures the inherent variability associated with seismic source, path and soil condition, etc.

In order to be compatible with the seismic scenario where this base-isolated RC frame is located, the ground motion suite is generated for the following seismic scenarios: moment magnitude M_w (6.5, 7.0, and 7.5), source-to-site distance R_{rup} (5, 10, and 15 km), medium-stiff soil class (shear wave velocity $V_{s,30}=300$, 400, and 500 m/s). Therefore, there are a total of 27 seismic scenarios, and 6 ground motions are generated for each scenario, amounting to 162 synthetic ground motions in total. It's worth noting that the number of this suite of synthetic ground motions far exceeds the minimum number of the required motions suggested by Pahlavan et al. (2016), indicating that these synthetic motions are sufficient to represent the salient features of NFFD ground motions in the region under consideration.

Comparisons between the design spectrum, mean and mean ± 1 standard deviation response spectra of these synthetic ground motions are presented in Fig. 5a. It is indicated that the mean response spectrum is approximately consistent with the design spectrum that accounts for near-fault effects. Whereas, the mean spectrum is observed to be slightly larger than the design spectrum in the range of 1–3.5 s, which can be attributed to the presence of velocity pulse in NFFD ground motions.

3.3 The selection of IM and EDPs

The selection of an optimal IM is a crucial part in seismic vulnerability assessment, and the corresponding metrics include practicality, efficiency, sufficiency, and hazard computability (Padgett et al. 2008). In this study, the issue regarding choosing the appropriate IM

is not further discussed. Based on the existing literatures (Guan et al. 2015; Hariri-Ardebili and Saouma 2016) and our preliminary analysis results, the spectral acceleration at the isolation period, $S_a(T_{iso}, 5\%)$, is selected as the IM parameter here. For brevity, $S_a(T_{iso}, 5\%)$ is simplified as S_a in the subsequent section. Figure 5b plots the distribution of S_a values for this suite of synthetic ground motions, and it is observed that this ground motion set covers a relatively broad range of S_a values.

The base-isolation layer and the superstructure are chosen as the two major vulnerable components of this structural system, and the damage states for the two ingredients are quantified in terms of corresponding EDPs. As stated in Sect. 3.1.2, the failure mode of LRBs is assumed to be dominated by the shear failure, and is quantitatively determined in terms of the maximum shear strain (γ_s), namely, $\gamma_s = u_b/T_r$, u_b is the lateral displacement, and T_r is the total thickness of rubber layers. The damage state for the superstructure is quantified by the maximum inter-story drift ratio θ_{IS}, i.e., $\theta_{IS} = u_{IS}/h$, u_{IS} denotes the inter-story drift, and h is the story height. Therefore, γ_s and θ_{IS} are the two selected EDPs in this system.

Given that this stochastic NFFD model is a single-component model (i.e., in the orientation of the strongest pulse within the horizontal plane), the IM and EDPs, as well as capacities, are all taken as one-component variables.

3.4 Limit state (capacity) models

Four levels of damage states are typically employed in the seismic fragility analysis (i.e., slight, moderate, extensive, and collapse), and are defined in terms of the selected EDPs. Based on recommendations from previous studies (Dezfuli and Alam 2017; Nielson and DesRoches 2007; Ramanathan et al. 2012), the coefficients of variation (COV) is utilized to characterize the uncertainty associated with each damage state. The smaller value of COV (i.e., 0.25) is assumed in slight and moderate damage states, and the relatively larger COV value (i.e., 0.5) is assigned in extensive and collapse limit states. The dispersion β_c is calculated as $\beta_c = \sqrt{\ln(1 + COV^2)}$, and the corresponding values of 0.24 and 0.47 are separately obtained. The distribution parameters for capacity models of these two components are given in Table 5. It's worth noting that the correlation of these component capacities is not considered, although the dependence among these component demands are incorporated in this study.

In the actual process of calculation, the maximum base displacement, $u_b = \gamma_s \times T_r$, and the maximum inter-story drift in the superstructure, $u_{IS} = \theta_{IS} \times h$, are utilized for convenience.

3.5 The establishment of JPSDM

For the sake of constructing the sampling-based JPSDM, first, the PSDM of each EDP_i is developed by the linear regression analysis; then, the best-fit copula for modeling the dependence structure of e_1 and e_2 in the two PSDMs is quantitatively identified in terms of

Table 5 Lognormal parameters for capacity models of the two components

i	EDP	LS_1		LS_2		LS_3		LS_4	
		$S_{c,1}$	$\beta_{c,1}$	$S_{c,2}$	$\beta_{c,2}$	$S_{c,3}$	$\beta_{c,3}$	$S_{c,4}$	$\beta_{c,4}$
1	γ_s	100%	0.24	150%	0.24	200%	0.47	250%	0.47
2	θ_{IS}	1/550	0.24	1/250	0.24	1/125	0.47	1/50	0.47

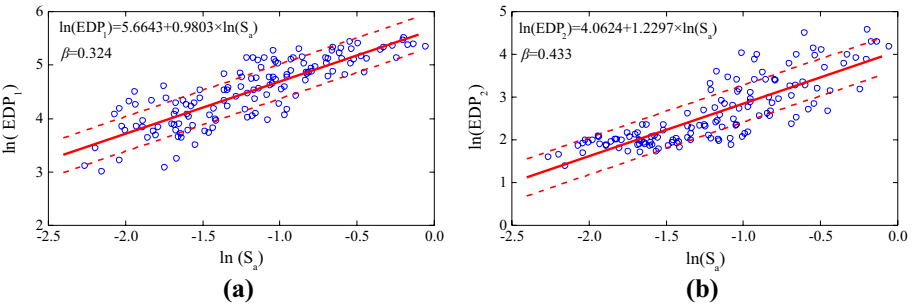

Fig. 6 PSDMs for different EDPs: **a** EDP_1; **b** EDP_2

Table 6 The regression parameters of PSDM for each component

i	a	b	$\beta_{EDP\|IM}$	R^2
$\ln(EDP_1)$	288.39	0.98	0.324	0.708
$\ln(EDP_2)$	58.11	1.23	0.433	0.681

AIC and BIC values; subsequently, the sampling-based JPSDM, which provides a large set of simulated samples of the two correlated EDPs under each IM level, is constructed based on the best-fit copula and the fitted conditional lognormal marginal distribution; finally, this JPSDM is utilized with the capacity models of these two components to estimate $P_{f,\mathrm{sys}}$ at each level of IM, and the MLE is adopted to obtain the system-level fragility function.

3.5.1 The PSDMs of multiple EDPs

Based on the structural model and the synthetic ground motions suite, 162 nonlinear time-history analyses are performed, and the maximum demand quantities, including the horizontal displacement in the base-isolation layer and the lateral drift of each floor, are recorded. It is found that the horizontal displacement demand is, to some extent, linearly distributed along the height of superstructure, as the seismic response is dominated by the first mode shape and, therefore, the displacement demand is concentrated in the base-isolation layer, due to the presence of laterally-flexible base-isolation layer. The maximum inter-story drift usually corresponds to that at the first story.

The linear regression analysis is performed, and the mean and mean $\pm$ 1 standard deviation of PSDMs in the log–log space for these two EDPs are plotted in Fig. 6. The estimated parameters (a_i, b_i, and $\beta_{EDP/IM,i}$) of PSDMs, as well as the coefficients of determination R^2, for the two considered EDPs are listed in Table 6, and the relatively larger value of R^2 implies that the linear regression in the log–log space for these two EDPs is reasonable.

Based on the two established PSDMs, the normal marginal distribution parameters ($\ln(S_{d,i})$, $\beta_{EDP|IM,i}$) of each $\ln(EDP_i)$, which is conditioned on the IM level, can be obtained easily. And it should be noted that the constant variance for the marginal distribution is assumed in the whole IM range.

To test the normality requirement of the residual term e_1 and e_2 in the two PSDMs, the quantile–quantile (Q–Q) plots of e_1 and e_2 are separately shown in Fig. 7a, b. In the Q–Q plot, the abscissa axis and the vertical axis represent the theoretical quantile values from a normal distribution and the quantile values of sample data, respectively. It is observed

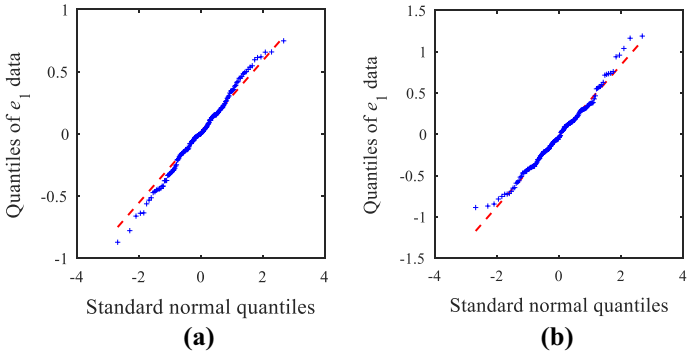

Fig. 7 Q-Q plots of the residual terms: **a** e_1, **b** e_2

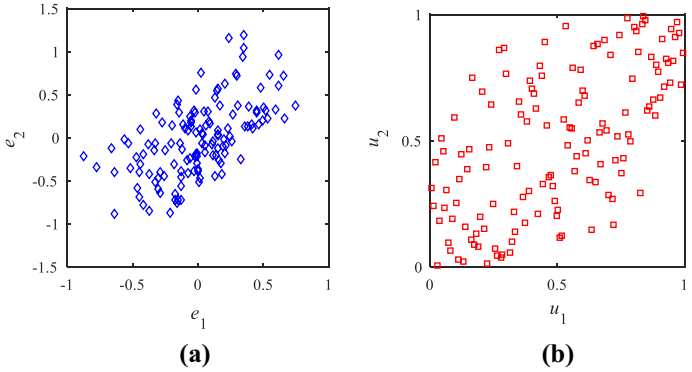

Fig. 8 Scatter plots of the residual term, e_1 and e_2, and their pseudo observations, u_1 and u_2: **a** e_1–e_2, **b** u_1–u_2

that these residual data are almost aligned with the diagonal line, confirming that the two residual terms e_1 and e_2 satisfy the normality requirement underlying the linear regression process.

3.5.2 Dependence modeling of multiple EDPs

The copula approach is employed to characterize the dependence structure of these two residual term, e_1 and e_2. First, to visually inspect the statistical characteristic of e_1 and e_2, scatter plots of e_1 and e_2 and those of their pseudo-observations, u_1 and u_2, are shown in Fig. 8a, b, respectively. Positive correlation and symmetry are observed in e_1–e_2 and u_1–u_2 data. Moreover, the upper and lower tail dependence of u_1 and u_2 data are also manifested to some extent. These observations indicate that the *t* copula is likely to be suitable for the considered residual data.

To quantitatively identify the best-fit copula for describing the correlation between e_1 and e_2, the five copula functions mentioned in Sect. 2.2.2.1 are fitted to the residual data by the MPLE method, and the estimated values of copula parameters for these five copulas are presented in Table 7. In addition, the estimated copula parameters based on the inversion

of Kendall's τ method are presented in parentheses in Table 7. It is found that the estimated copula parameters based on these two methods are almost identical, infirming the reasonability of these two methods being used. And the estimated copula parameters values from the MPLE method is further used in the subsequent part.

As presented in Table 7, the goodness-of-fit of these five candidate copulas is examined in terms of AIC and BIC values, and the minimum values of AIC and BIC are marked as bold. It is observed that the t copula is quantified as the best-fit copula among these copulas, corresponding to the minimum value of both AIC and BIC. However, the difference between Gaussian and t copula in terms of AIC and BIC values is insignificant, indicating the similar modeling capacity of these two copulas. This behavior can also be reflected by the relatively large estimated value of the degrees-of-freedom parameter v in the t copula, given that Gaussian copula corresponds to the t copula with $v=\infty$.

The left column in Fig. 9 compares the original data (162 samples) with the simulated data (5×10^5 samples) of u_1 and u_2 for the five candidate copulas based on their fitted copula parameters. It is found that the simulating capacity of the Clayton copula is the worst, which is distinctly reflected by the fact that more simulated samples are observed in the upper-left and the lower-right corners. The inferior behavior of the Clayton copula is also manifested by the maximum AIC and BIC values among these five copulas in the model selection. The t, Gaussian, and Frank copulas simulate the original residual data better, and their AIC and BIC values are relatively similar. However, as mentioned in Sect. 2.2.2.1, the Gaussian and Frank copulas cannot represent the upper and lower tail dependence of the considered data. The observation in Fig. 9c indicates that the performance of the best-fit t copula for describing the dependence between u_1 and u_2 is satisfactory, as it effectively characterizes both the symmetry and the tail dependence of u_1–u_2.

Furthermore, to test the overall simulating capacity for the joint probability characteristics of the two residual terms e_1 and e_2, the original data (blue) and the simulated data (black) of e_1 and e_2 based on both the five fitted copula functions and the fitted normal marginal distributions are compared in the right column in Fig. 9. It is noted that $e_i \sim N(0, \beta_{\mathrm{EDP|IM},i})$, $(i=1, 2)$, and the simulated samples of e_i are obtained by the isoprobabilistic transformation of those of u_i, namely, $e_i = \Phi_i^{-1}(u_i)$, where $\Phi_i^{-1}()$ is the respective inverse CDF of e_i.

Similarly, the better simulating performance of t copula is observed by comparison with other copulas. It should be pointed out that the simulated results of u_1–u_2 are solely dominated by the copula modeling, however, the simulated results of e_1–e_2 are influenced by both the marginal distribution fitting and the copula modeling. It can be concluded that the combination of t copula, which is quantitatively identified as the best-fit copula function for the dependence modeling, and the normal marginal distribution, which is required in the linear

Table 7 The obtained AIC and BIC values for the candidate copulas

Copula	Estimated parameters	AIC	BIC
Gaussian	$\rho=0.6398$ (0.6412)	−59.21	−56.31
t	$\rho=0.6488$ (0.6412)	**−59.36**	**−56.45**
	$v=192.4$ (192.5)		
Gumbel	$\theta=1.7897$ (1.8164)	−49.49	−46.58
Clayton	$\theta=1.2918$ (1.2743)	−36.07	−33.16
Frank	$\theta=4.8957$ (4.886)	−56.84	−53.93

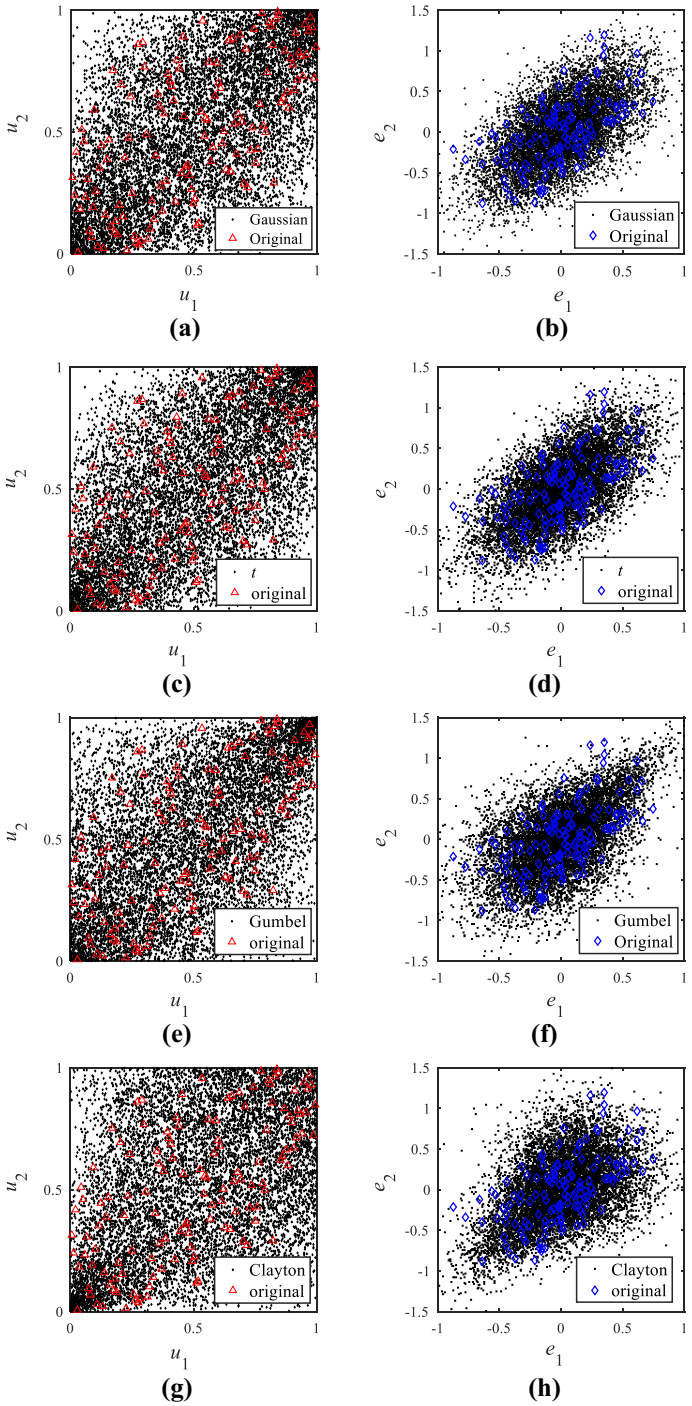

Fig. 9 Comparison between the original data and the simulated data of u_1–u_2 and e_1–e_2 based on different copulas: **a** Gaussian (u_1–u_2), **b** Gaussian (e_1–e_2), **c** t (u_1–u_2), **d** t (e_1–e_2), **e** Gumbel (u_1–u_2), **f** Gumbel (e_1–e_2), **g** Clayton (u_1–u_2), **h** Clayton (e_1–e_2), **i** Frank (u_1–u_2), **j** Frank (e_1–e_2)

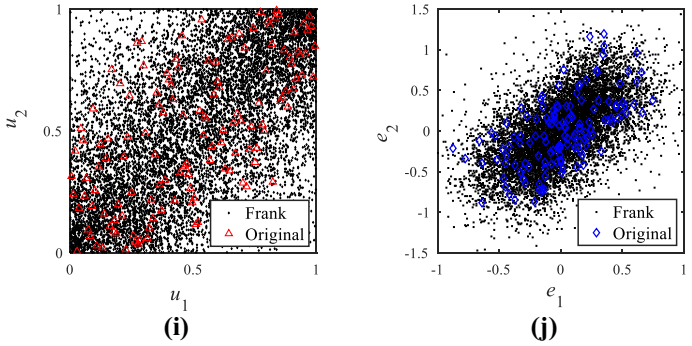

Fig. 9 (continued)

regression analysis, can reasonably describe the joint probability distribution of the two residual terms, e_1 and e_2.

Therefore, both the best-fit *t* copula and the lognormal marginal distribution, which is conditioned on the IM level, are capable of representing the conditional joint probability characteristics of the two considered EDPs under each level of IM, and are further employed to establish the sampling-based JPSDM in the subsequent section.

3.6 System fragility curves

According to Sect. 2.2.3, the sampling-based JPSDM, which generates a large set of simulated samples for the two correlated EDPs under each level of IM, is constructed based on the combination of the best-fit *t* copula function and their respective conditional lognormal marginal distributions. Under the assumption of a serial system, the system-level fragility curve can be generated by virtue of both the established JPSDM and capacity models of these two considered components (Sect. 2.2.4). Figure 10 presents the overall system fragility curves under different damage states.

Based on the formulation presented in Eq. (6), the component-level fragility curves at different damage states are developed, which not only reflect the relative vulnerability of different components, but also provide insights into the most vulnerable component in the system. As presented in Fig. 10, the shift in the vulnerability of components is observed with the change of damage states. In the slight and moderate damage states, the vulnerability of the superstructure is more significant than that of the base-isolation layer; and the similar fragility contributions of these two components are observed in the extensive damage state; whereas, the bearing response dominates the system vulnerability in the complete damage state. Comparisons between the system-level and the two component-level fragility curves under various damage states show that the system-level fragility is more significant than that of any individual component, which is attributed to the underlying assumption of the serial system in this study.

For comparison, the first-order reliability bounds of the system-level fragility $P_{f,\mathrm{sys}}$ is calculated in terms of the component-level fragility, $P_{f,i}$ ($i=1, \ldots, n$), and are given as follows (Ezzeldin et al. 2017):

$$\max_{i=1}^{n}\left(P_{f,i}\right) \le P_{f,\mathrm{sys}} \le 1-\prod_{i=1}^{n}\left(1-P_{f,i}\right) \tag{22}$$

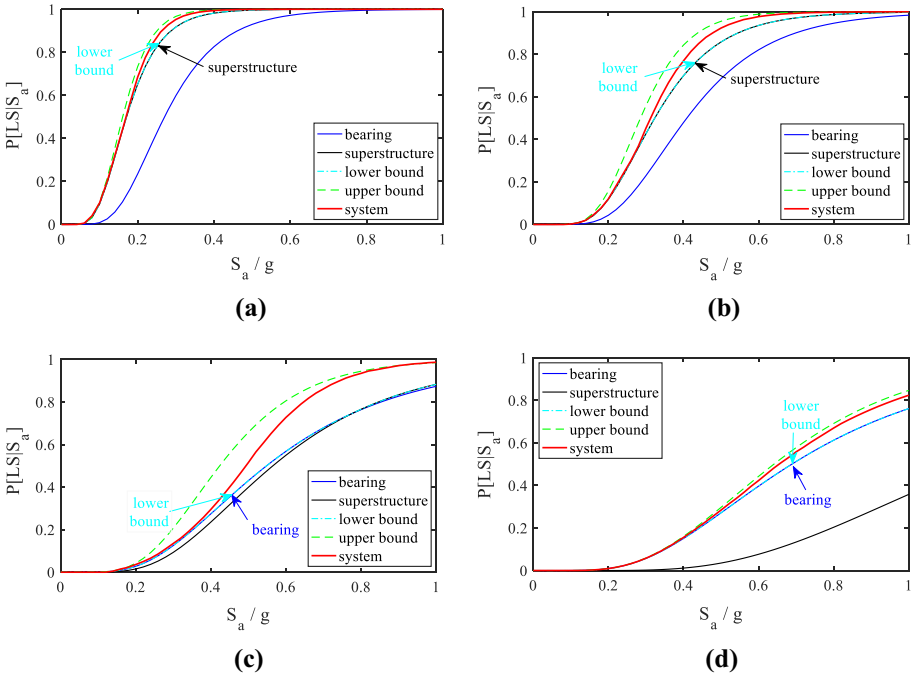

Fig. 10 The system- and component- level fragility curves, as well as the first-order bounds, under different limit states: **a** slight, **b** moderate, **c** extensive, **d** complete

where the lower bound corresponds to the maximum component fragility, assuming the complete correlation between different components; whereas, the upper bound assumes the independence among various components. The first-order bounds for the system-level fragility curves in different limit states are presented in Fig. 10 as well. It is found that the lower bound coincides with the fragility curve of the superstructure in slight and moderate damage states, as the superstructure governs the system fragility under these two damage states; whereas, the lower bound corresponds to the fragility of bearing in the other two damage states. The system-level fragility curve is located in the interval between the upper and lower bounds, and the discrepancy between the upper and lower bounds is dominated by the relative fragility contributions of different components. In the extensive damage state, the base-isolation layer and the superstructure have similar fragility contributions, and the gap between the bounds is relatively distinct. Under that circumstance, it is vital to directly generating system-level fragility curve based on the proposed methodology, rather than using the first-order bounds. Whereas, the relatively narrow bounds are observed in the other three limit states, due to the existence of the predominantly fragile component.

Moreover, the system-level fragility curve is observed to be closer to the upper bound in the range of higher IM level, denoting the independence between the two components. However, the estimated value of Kendall's τ coefficient between these two components based on the original data set is 0.4495, indicating the existence of relatively medium correlation. This discrepancy may be attributed to the fact that there is a relatively smaller number of observed e_1–e_2 data in the higher IM level, giving rise to the inaccuracy of estimating system-level fragility to some extent.

To investigate the impact of different copulas selection on the development of the overall system fragility, comparisons between fragility curves derived from the five copula functions are illustrated in Fig. 11. It is observed that the influence of different copulas on the system-level fragility varies depending on the damage state of interest. In essence, this observed behavior is also attributed to the relative fragility of different components. At the extensive damage state, the vulnerability contribution of the base-isolation layer is similar to that of the superstructure (as seen in Fig. 10c), and the difference between these five copulas is relatively larger. In that case, the quantitative identification of the best-fit copula function for modeling the dependence among multiple EDPs is essential to the accuracy of the system-level fragility. Whereas, in the remaining three damage states, accounting for the existence of predominantly-vulnerable component, the discrepancy of system-level fragility curves using different copulas is relatively subtle. Moreover, the methodology proposed by Nielson and DesRoches (2007) are constructed based on the Nataf transformation, which essentially corresponds to the Gaussian copula dependence structure (Lebrun and Dutfoy 2009). Though the difference of the system-level fragility between the Gaussian copula and best-fit t copula is slight in this case study, the proposed method quantitatively identifies the best-fit copula among candidate copulas without suffering from the restriction of the inherent Gaussian copula assumption in Nielson and DesRoches (2007), and is a more flexible and general approach to develop the fragility curves at the system level.

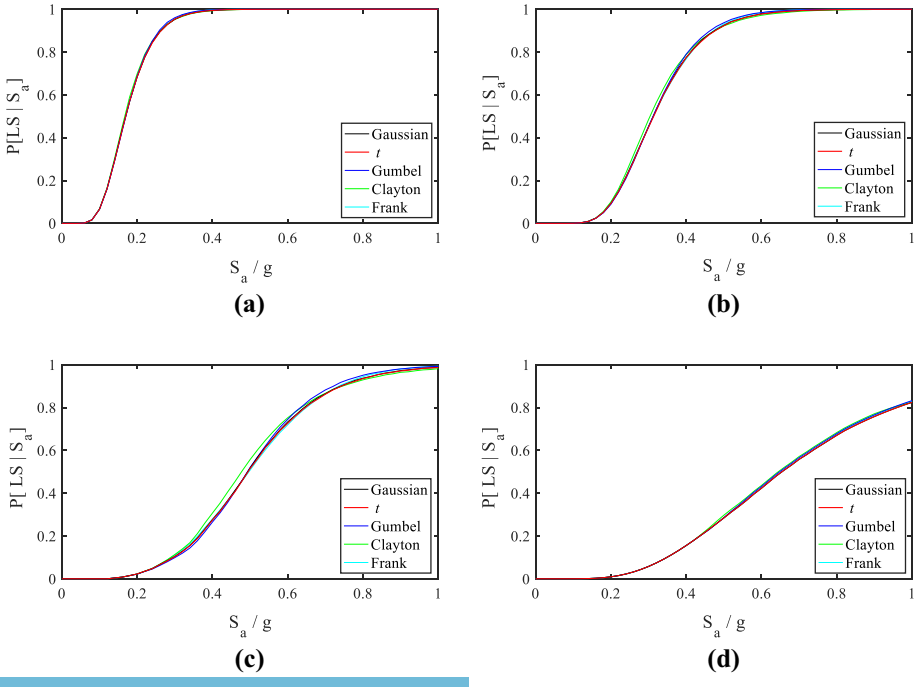

Fig. 11 Comparison of system-level fragility curves derived from different copula functions at various damage states: **a** slight, **b** moderate, **c** extensive, **d** complete

4 Conclusions

This study investigates the seismic vulnerability of base-isolated structures under NFFD ground motions, and the emphasis of this study is placed on proposing a general framework for deriving the system-level fragility via the copula approach. In this framework, to account for the vulnerability contributions of multiple correlated components, the JPSDM is constructed, where the copula function is utilized to characterize the dependence structure among multiple component demands, and the overall system fragility is eventually generated based on both the established JPSDM and the capacity models of these considered components. In the case study of a typical base-isolation RC frame, the maximum lateral displacement in the base-isolation layer and the peak inter-story drift in the superstructure are simply selected as the two major component demands. Comparisons between the system-level and component-level fragility curves, as well as the upper and lower first-order bounds, are made. Furthermore, the impact of selecting different copulas on the overall system fragility is investigated. Main conclusions are drawn as follows:

(1) Based on the metrics of both AIC and BIC values, the *t* copula is quantitatively identified as the best-fit copula for modeling the dependence among the two residual terms e_1 and e_2 in each PSDM, as it effectively captures the symmetry and the tail dependence. Therefore, the combination of the best-fit *t* copula and the fitted lognormal marginal distributions, which are conditioned on the IM level, is capable of representing the joint probability distribution of these two EDPs under each level of IM, and is further utilized in the construction of sampling-based JPSDM.
(2) The shift in the fragility of components is observed with the change of four damage states, and the seismic fragility of the system is more significant than that of any individual component. When multiple components have similar fragility contributions, the discrepancy between the upper and lower first-order bounds is significant; under that circumstance, it is crucial to directly derive the system-level fragility curves based on the proposed methodology, rather than estimating it by the first-order bounds. Whereas, the width of the upper and lower bounds is relatively smaller in the other three damage states, as the existence of the predominantly-fragile component.
(3) The impact of different copulas selection on the development of system-level fragility curve is essentially dominated by the relative fragility of different components. When multiple components have similar fragility contributions, the difference among various copulas is slightly greater; in that case, the quantitative identification of the best-fit copula function is of vital importance to the accuracy of the system-level fragility curves.

It should be noted that the analysis results are mainly related to the considered structure type, the number and type of structural components, and the earthquake characteristic, etc. Whereas, this general framework proposed in this study for developing the system-level fragility still holds, when the vulnerability contributions of multiple correlated components in the system are incorporated. Furthermore, this copula-based framework can be easily extended to the case where the non-lognormal marginal distributions are encountered, and this flexibility is attributed to the separation of marginal modeling and the dependence modeling in the copula method.

Acknowledgements This research was supported by the National Natural Science Foundation of China (Grant No. 51438002).

References

Akaike H (1974) A new look at the statistical model identification. IEEE Trans Autom Control 19:716–723. https://doi.org/10.1109/TAC.1974.1100705

Alhan C, Öncü-Davas S (2016) Performance limits of seismically isolated buildings under near-field earthquakes. Eng Struct 116:83–94. https://doi.org/10.1016/j.engstruct.2016.02.043

Baker JW (2015) Efficient analytical fragility function fitting using dynamic structural analysis. Earthq Spectra 31:579–599. https://doi.org/10.1193/021113EQS025M

Bray JD, Rodriguez-Marek A (2004) Characterization of forward-directivity ground motions in the near-fault region. Soil Dyn Earthq Eng 24:815–828. https://doi.org/10.1016/j.soildyn.2004.05.001

Buckle IG, Constantinou MC, Diceli M, Ghasemi H (2006) Seismic isolation of highway bridges. Report MCEER-06-SP07, Multidisciplinary Center for Earthquake Engineering Research, The State University of New York, Buffalo, USA

Casciati F (1989) Stochastic dynamics of hysteretic media. Struct Saf 6:259–269. https://doi.org/10.1016/0167-4730(89)90026-x

Constantinou M, Mokha A, Reinhorn A (1990) Teflon bearings in base isolation II: modeling. J Struct Eng 116:455–474. https://doi.org/10.1061/(ASCE)0733-9445(1990)116:2(455)

Cornell CA, Jalayer F, Hamburger RO, Foutch DA (2002) Probabilistic basis for 2000 SAC federal emergency management agency steel moment frame guidelines. J Struct Eng 128:526–533. https://doi.org/10.1061/(ASCE)0733-9445(2002)128:4(526)

Dezfuli FH, Alam MS (2017) Effect of different steel-reinforced elastomeric isolators on the seismic fragility of a highway bridge. Struct Control Health Monit 24:e1866. https://doi.org/10.1002/stc.1866

Dickinson BW, Gavin HP (2011) Parametric statistical generalization of uniform-hazard earthquake ground motions. J Struct Eng 137:410–422. https://doi.org/10.1061/(ASCE)ST.1943-541X.0000330

Eckernkemper T (2018) Modeling systemic risk: time-varying tail dependence when forecasting marginal expected shortfall. J Financ Econom 16:63–117. https://doi.org/10.1093/jjfinec/nbx026

Erdik M (2017) Earthquake risk assessment. Bull Earthq Eng 15:5055–5092. https://doi.org/10.1007/s10518-017-0235-2

Ezzeldin M, Wiebe L, El-Dakhakhni W (2017) System-level seismic risk assessment methodology: application to reinforced masonry buildings with boundary elements. J Struct Eng 143:04017084. https://doi.org/10.1061/(ASCE)ST.1943-541X.0001815

Filippou FC, Bertero VV, Popov EP (1983) Effects of bond deterioration on hysteretic behavior of reinforced concrete joints. Report EERC 83-19, Earthquake Engineering Research Center, University of California, Berkelery, USA

Genest C, Favre AC (2007) Everything you always wanted to know about copula modeling but were afraid to ask. J Hydrol Eng 12:347–368. https://doi.org/10.1061/(ASCE)1084-0699(2007)12:4(347)

Guan M, Du H, Cui J, Zeng Q, Jiang H (2015) Optimal ground motion intensity measure for long-period structures. Meas Sci Technol 26:105001. https://doi.org/10.1088/0957-0233/26/10/105001

Hariri-Ardebili MA, Saouma VE (2016) Probabilistic seismic demand model and optimal intensity measure for concrete dams. Struct Saf 59:67–85. https://doi.org/10.1016/j.strusafe.2015.12.001

Huang WH (2002) Bi-directional testing, modeling, and system response of seismically isolated bridges. Ph.D. Dissertation, University of California, Berkeley, USA

Kim S-H, Shinozuka M (2004) Development of fragility curves of bridges retrofitted by column jacketing. Probab Eng Mech 19:105–112. https://doi.org/10.1016/j.probengmech.2003.11.009

Kim G, Silvapulle MJ, Silvapulle P (2007) Comparison of semiparametric and parametric methods for estimating copulas. Comput Stat Data Anal 51:2836–2850. https://doi.org/10.1016/j.csda.2006.10.009

Kojadinovic I, Yan J (2010) Comparison of three semiparametric methods for estimating dependence parameters in copula models. Insur Math Econ 47:52–63. https://doi.org/10.1016/j.insmatheco.2010.03.008

Kumar M, Whittaker AS, Constantinou MC (2015) Experimental investigation of cavitation in elastomeric seismic isolation bearings. Eng Struct 101:290–305. https://doi.org/10.1016/j.engstruct.2015.07.014

Lebrun R, Dutfoy A (2009) An innovating analysis of the Nataf transformation from the copula viewpoint. Probab Eng Mech 24:312–320. https://doi.org/10.1016/j.probengmech.2008.08.001

Liu PL, Der Kiureghian A (1986) Multivariate distribution models with prescribed marginals and covariances. Probab Eng Mech 1:105–112. https://doi.org/10.1016/0266-8920(86)90033-0

Luco N, Bazzurro P (2007) Does amplitude scaling of ground motion records result in biased nonlinear structural drift responses? Earthq Eng Struct Dyn 36:1813–1835. https://doi.org/10.1002/eqe.695

Mathworks (2018) Statistics and machine learning toolbox. https://ww2.mathworks.cn/help/matlab/

McKenna F, Fenves GL, Scott MH (2000) Open system for earthquake engineering simulation (OpenSees). University of California, Berkeley, USA

Ministry of Housing and Urban-Rural Development of the People's Republic of China (2010) Code for Seismic Design of Buildings (GB 50011-2010). Chinese Architecture & Building Press, Beijing
Mohd Yassin MH (1994) Nonlinear analysis of prestressed concrete sructures under monotonic and cyclic loads. Ph.D. Dissertation, University of California, Berkeley, USA
Montuori GM, Mele E, Marrazzo G, Brandonisio G, De Luca A (2016) Stability issues and pressure–shear interaction in elastomeric bearings: the primary role of the secondary shape factor. Bull Earthq Eng 14:569–597. https://doi.org/10.1007/s10518-015-9819-x
Murcia-Delso J, Shing PB (2012) Fragility analysis of reinforced masonry shear walls. Earthq Spectra 28:1523–1547. https://doi.org/10.1193/1.4000075
Nelsen RB (2006) An introduction to copulas. Springer, New York
Nielson BG, DesRoches R (2007) Seismic fragility methodology for highway bridges using a component level approach. Earthq Eng Struct Dyn 36:823–839. https://doi.org/10.1002/eqe.655
Noh HY, Lallemant D, Kiremidjian AS (2015) Development of empirical and analytical fragility functions using kernel smoothing methods. Earthq Eng Struct Dyn 44:1163–1180. https://doi.org/10.1002/eqe.2505
Padgett JE, Nielson BG, DesRoches R (2008) Selection of optimal intensity measures in probabilistic seismic demand models of highway bridge portfolios. Earthq Eng Struct Dyn 37:711–725. https://doi.org/10.1002/eqe.782
Pahlavan H, Zakeri B, Amiri GG, Shaianfar M (2016) Probabilistic vulnerability assessment of horizontally curved multiframe RC box-girder highway bridges. J Perform Constr Facil 30:04015038. https://doi.org/10.1061/(ASCE)CF.1943-5509.0000780
Ramanathan K, DesRoches R, Padgett JE (2012) A comparison of pre- and post-seismic design considerations in moderate seismic zones through the fragility assessment of multispan bridge classes. Eng Struct 45:559–573. https://doi.org/10.1016/j.engstruct.2012.07.004
R Development Core Team (2018) R: a language and environment for statistical computing. R foundation for statistical computing. Vienna, Austria. http://www.r-project.org
Rezaeian S, Der Kiureghian A (2008) A stochastic ground motion model with separable temporal and spectral nonstationarities. Earthq Eng Struct Dyn 37:1565–1584. https://doi.org/10.1002/eqe.831
Rosenblatt M (1952) Remarks on a multiformation. Ann Math Stat 23:470–472. https://doi.org/10.1214/aoms/1177729394
Sato E, Furukawa S, Kakehi A, Nakashima M (2011) Full-scale shaking table test for examination of safety and functionality of base-isolated medical facilities. Earthq Eng Struct Dyn 40:1435–1453. https://doi.org/10.1002/eqe.1097
Schellenberg AH, Sarebanha A, Schoettler MJ, Mosqueda G, Benzoni G, Mahin SA (2015) Hybrid simulation of seismic isolation systems applied to an APR-1400 nuclear power plant. Report PEER 2015/05 Pacific Earthquake Engineering Research Center (PEER), University of California, Berkelery, USA
Schwarz G (1978) Estimating the dimension of a model. Ann Stat 6:461–464. https://doi.org/10.1214/aos/1176344136
Shahi SK, Baker JW (2014) An efficient algorithm to identify strong-velocity pulses in multicomponent ground motions. Bull Seismol Soc Am 104:2456–2466. https://doi.org/10.1785/0120130191
Shi Y, Kurata M, Nakashima M (2014) Disorder and damage of base-isolated medical facilities when subjected to near-fault and long-period ground motions. Earthq Eng Struct Dyn 43:1683–1701. https://doi.org/10.1002/eqe.2417
Sklar A (1959) Fonctions de répartition à n dimensions et leurs marges. Publ Inst Statist Univ Paris 8:229–231
Tosunoglu F, Singh VP (2018) Multivariate modeling of annual instantaneous maximum flows using copulas. J Hydrol Eng 23:04018003. https://doi.org/10.1061/(ASCE)HE.1943-5584.0001644
Wang F, Li H (2017) Towards reliability evaluation involving correlated multivariates under incomplete probability information: a reconstructed joint probability distribution for isoprobabilistic transformation. Struct Saf 69:1–10. https://doi.org/10.1016/j.strusafe.2017.07.002
Wang QA, Wu Z, Liu S (2018) Multivariate probabilistic seismic demand model for the bridge multidimensional fragility analysis. KSCE J Civ Eng. https://doi.org/10.1007/s12205-018-0414-y
Warn GP, Whittaker AS, Constantinou MC (2007) Vertical stiffness of elastomeric and lead-rubber seismic isolation bearings. J Struct Eng 133:1227–1236. https://doi.org/10.1061/(ASCE)0733-9445(2007)133:9(1227)
Wu XZ (2013) Probabilistic slope stability analysis by a copula-based sampling method. Comput Geosci 17:739–755. https://doi.org/10.1007/s10596-013-9353-3

Wu W, Li L, Shao X (2016) Seismic assessment of medium-span concrete cable-stayed bridges using the component and system fragility functions. J Bridge Eng 21:04016027. https://doi.org/10.1061/(ASCE)BE.1943-5592.0000888

Yan J (2007) Enjoy the joy of copulas: with a package copula. J Stat Softw 21:1–21. https://doi.org/10.18637/jss.v021.i04

Zentner I (2017) A general framework for the estimation of analytical fragility functions based on multivariate probability distributions. Struct Saf 64:54–61. https://doi.org/10.1016/j.strusafe.2016.09.003

Zentner I, Gündel M, Bonfils N (2017) Fragility analysis methods: review of existing approaches and application. Nucl Eng Des 323:245–258. https://doi.org/10.1016/j.nucengdes.2016.12.021

Zhang J, Huo Y (2009) Evaluating effectiveness and optimum design of isolation devices for highway bridges using the fragility function method. Eng Struct 31:1648–1660. https://doi.org/10.1016/j.engstruct.2009.02.017

Zhou T, Wu YF, Li AQ (2018) Stochastic modeling and synthesis of near-fault forward-directivity ground motions. KSCE J Civ Eng **(in press)**